PERCEPTIVE SENSOR MONITORING ANALYSIS OF INTELLIGENT STRUCTURE MORPHOLOGY

Yang ZHONGGUO[1], Cai TIANFANG[2]

In order to solve a problem that the characteristics of space plate structure is easy to result in changing structure morphology and dramatic low-frequency vibration after the structure is impacted by space environment and incentive disturbance. Based on the intelligent surface structure of distributed Fiber Bragg Grating (FBG) sensor network, the paper designs the framework of the sensor network, optimizes FBG sensor network of layout to acquire change information of structure morphology. Then, based on fitting reconstruction method, the paper realizes morphological real-time perception and reconstruction of platy structure and realizes dynamic expression and far-field monitoring through spot visualization technology. The experiment shows that the method is feasible and has great evaluation effects.

Keywords: Intelligent Structure, Sensor, Perception, Reconstruction.

1. Introduction

Multiple, extensive and networked information perception is the important foundation on unifying collaborative management and scientific sustainable development of urban traffic in the future. Efficient and reasonable perceptive system can provide all-around data support for comprehensive operation management of urban traffic [1, 2, 3]. Establishment of perfect perceptive system and sensor network [4, 5] can promote traffic informationization and industrial integration effectively and speed up convenient [6, 7], safe, efficient and economic comprehensive system development for various items. Therefore, implementation technique study [8, 9, 10], performance evaluation study, and state optimization study etc., problems on perceptive system and sensor network become the key and difficult points in the future information acquisition field and play important theoretical significance and realistic guiding role on studying these problems.

Large-scale planar structure is the basic part that is widely applied to industrial field, especially for aerospace field. The planar structure generally is

[1] College of Mechanical and Electrical Engineering, Zaozhuang Institute, Zaozhuang, 277160, China, Emails: 13589610269@163com
[2] College of Mechanical and Electrical Engineering, Zaozhuang Institute, Zaozhuang, 277160, China

equipped with some characteristics, including light structure materials [11, 12], larger are, lower rigidness, small vibration damping, lower resonant frequency and multiple model response. Moreover, under the state of continuous work, it needs to continue to ensure higher running accuracy. Especially for maintaining structure shape, it has extremely rigorous technical requirements. Intelligent surface structure based on the distributed Fiber Bragg Grating sensor network is an important research direction of exploring the above-mentioned problems. The basic idea is to acquire change information of structure morphology by optimizing FBG sensor network of lay out. Then, based on the fitting reconstruction method structure morphology, the paper realizes morphological real-time perception and reconstruction of planar structure and realizes dynamic expression and far-field monitoring through spot visualization technology. Therefore, exploration and research of related technical methods have important scientific value, innovative significance and application prospect [13, 14].

2. Dynanic Monitoring Based on Optical Fiber Sensing Technology

In existing various FBG sensors, some of belong to static measurement sensor, such as temperature sensor, displacement sensor, and pressure sensor, etc. Signals measured by the sensor can display physical quantity of equipment under test directly after calibration. For example, wave length signals measured by the temperature sensor can display temperature of the measured position directly after calibration and can be used for judgment of conclusions. Some of them belong to dynamic signal measurement sensor [15, 16, 17], such as vibrating sensor (displacement, speed and acceleration). Though detection signals can display instant quantity of equipment after calibration, the instant quantity is not enough to display running status of the equipment but needs more follow-up processing.

In dynamic strain of mechanical equipment, most of them are existed in the form of periodic strain, because equipment, such as turbine, is rotary machinery and its loads are changed in line with certain requirements. The change requirements of periodic dynamic strain signals can be expressed by using the mathematic form:

$$\varepsilon(t + nT) = \varepsilon(t) \tag{1}$$

In the formula, T is changing period, and n is any integer.

In the measurement of FBG sensor on mechanical equipment, there is a sensor that is used for extracting vibration signals, such as FBG acceleration sensor. Moreover, strain sensor measurement can be divided into static strain measurement and dynamic strain measure, due to different measurement position and equipment characteristics.

When dynamic strain measurement is conducted in FBG of single mode fiber, the general disturbance index along the direction of FBG can be expressed as:

$$\Delta n_i(z,t) = \Delta n_0[1+\cos(\frac{2\pi}{\Lambda_i} z + \varphi_i(z,t))] \tag{2}$$

Where, z is the axial strain direction of grating, t is time coordinate, Δn_0 is the average index change space exceeding grading period "dc", $\varphi_i(z,t)$ is the phase increase caused by grating strain. The subscript is corresponding to the grating utilized in the equipment measurement.

In the dynamic linear strain process, reflectance spectrum of FBG is symmetrical in central wavelength. Therefore, the dependency of wavelength shift on dynamic strain can be written into:

$$\Delta\lambda_B(z_{mid},t) = \lambda_B(1-p_e)\varepsilon(z_{mid},t) \tag{3}$$

Where, $\varepsilon(z_{mid},t)$ is the dynamic strain of points in grating.

The analog signal collected from the sensor is passed through analog-digital conversion processing system and is transformed into numerical sequence. Digital signal is described as time function. Time-domain signal is the synthesis of entire equipment signal. Therefore, time-domain analysis is mainly used for observing running state of mechanical equipment in real time, but it can't reflect fault reasons of equipment. Common time-domain analysis methods mainly include wavelength analysis, shaft centerline orbit, synchronous mean and start-stop instant analysis, etc.

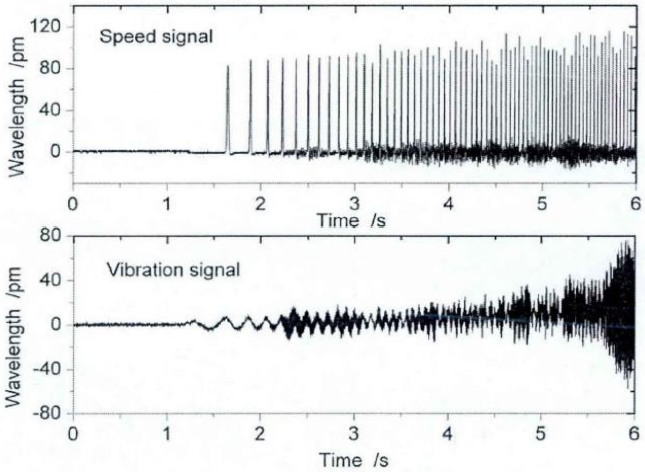

Fig. 1. Time-domain Signal of Start-stop Machine

As shown in Fig. 1, instant vibration of structure occurs in instant excitation force (which might be single-pulse or short-term oscillation excitation). When excitation stops, structure tends to its inherent frequency vibration. System damping results in exponential damping. Therefore, after stopping excitation force, time course of structure response is the sine wave set of damping. Because recombined wave of inherent modal superposition in the system is motivated by instant force, generally speaking damping of higher frequency component is relatively rapid. Higher frequency modal damping rapidly reduces vibration amplitudes. Synthetic waveform is degraded as the damping sinusoidal response of lowest frequency modes.

Applying Fourier transform is a basic technique that changes broadband time graphics into discrete frequency or frequency band. It is a kind of mathematical method that identifies sine components of constituting overall vibration signal. These sinusoidal signals include any possible machinery or electrical noise. In mechanical low-speed operation, it is impossible for equipment vibration to form simple harmonic motion, due to existence of various assembly errors. After time-domain signal is transformed in frequency signal by FFT, it can be found that there is frequency signal that has integral relations with fundamental signal, namely harmonic signal or frequency doubling signal, except for fundamental signal that is consistent with rotary frequency. Figure 2 is the frequency signal of bearing vibration measurement. It can be observed that there is clear existence of frequency doubling signal.

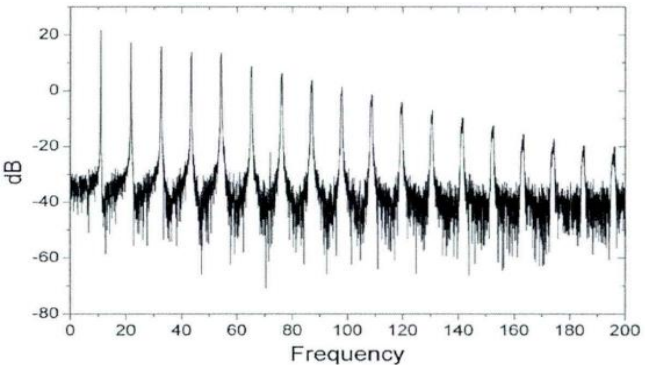

Fig. 2. Harmonic Frequency Characteristics

3. Sensor Network Experiment Structure Design

The system that is used for intelligent structure state monitoring has numerous similarities with other monitoring system distributions in overall composition, but it also has its own difference and characteristics. Macroscopically, it generally should

contain several modules, including detection module, data acquisition module, data processing module, data analysis module, real-time display and alarm module and state evaluation module. Based on FBG technology's real-time online detection of mechanized equipment, the monitoring system is constructed in line with its characteristics.

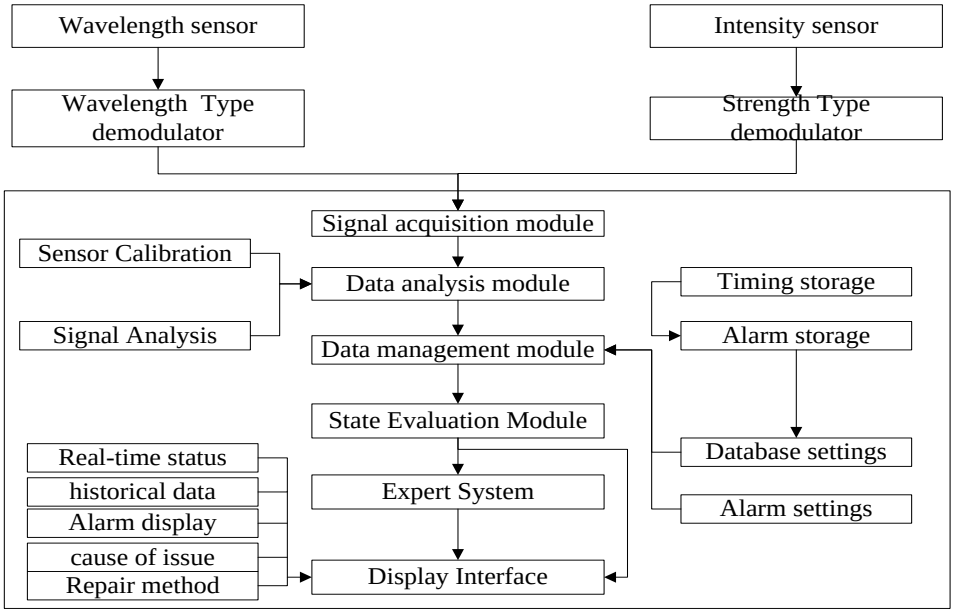

Fig. 3. Monitoring System Chart

According C/S framework and software functions, design software structure is shown in Fig. 4.

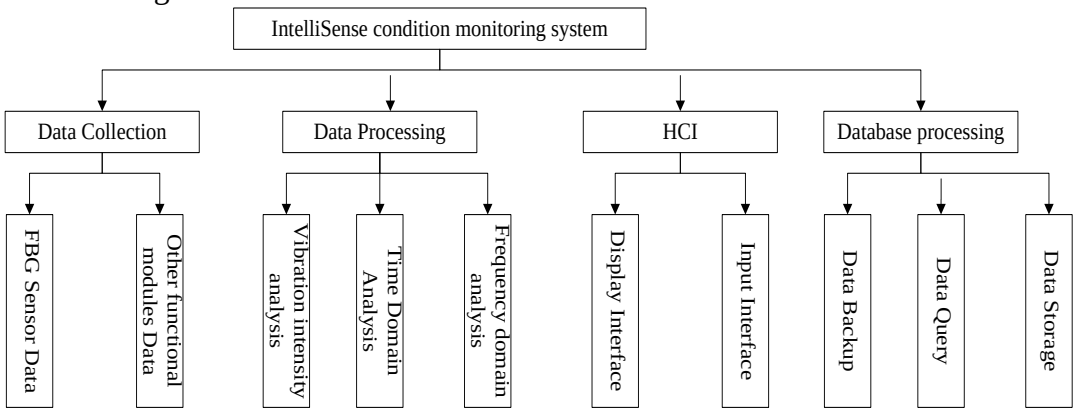

Fig. 4. System Software Structure

4. Intelligent Structure Perceptive Reconstruction Algorithm Based on Orthogonal Curve

The main analysis of plane curve reconstruction method is shown as follows: Assuming that the arc length is short enough, the length of each segment is arc. Because curvature is the reciprocal of circle radio, radio by radius can be obtained in line with arc curvature K (N_0):

$$R_0 = 1/K(N_0) \tag{4}$$

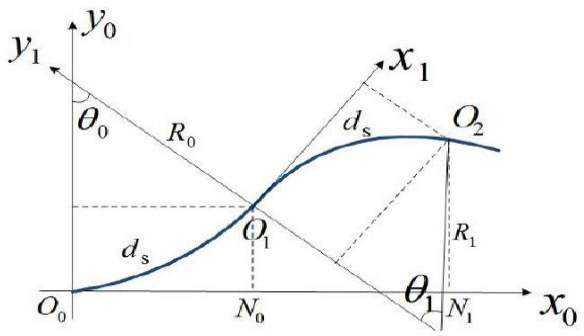

Fig. 5 Plane Curve Fitting Principle Analysis

Because the corresponding central angle of arc length is the specific value between arc length and radio, it can be obtained:

$$\theta_0 = S(N_0)/R_0 \tag{5}$$

Thus, it can be obtained from the figure that arc end node O_1 has the position coordinates in x_0, y_0 coordinate system, as follows:

$$(x_1 \quad y_1) = (R_0 \sin\theta_0 \quad R_0 \cos\theta_0) \tag{6}$$

(1) In transform coordinate system, the first arc node axle by axis and is marked as x_1 axle; Through O_1 and the vertical direction of x_1 axle, it is regarded as y axle and is marked as y_1 axle; With the true origin of O_1, x1 and y1 axles constitute the new coordinate(x_1, y_1);

(2) In the coordinate system (x_1, y_1) , end node O_1 is regarded as the starting node and new node O_2 is regarded as the new end node. The same method is used to

fit the second arc curve. The position coordinate of node O_2 in the position of (x_1, y_1) coordinate system can be obtained;

(3) In order to acquire the coordinate position of node O_2 in the basic coordinate system (x_0, y_0), the position coordinate in (x_1, y_1) and coordinate system must be translated into the coordinate position of basic coordinate system through the geometrical relationship. The coordinate system (x_1, y_1) can be regarded as the counterclockwise rotation θ_0 at the origin O_0, and the coordinate origin is moved to O_1. On the contrary, after (x_1, y_1) coordinate system moves the origin from O_1 to O_2, coordinate system is rotated in clockwise and changed into (x_0, y_0) coordinate system with θ_0. According to coordinate rotary formulate(6), it is easy to acquire the coordinate position in the original coordinate system.

(4) After acquiring the position coordinate of O_1 and O_2 in the fixed coordinate system (x_0, y_0), it can realize the reconstruction of curve through the way of connecting points.

If the first grating detection point of detection module is regarded as the origin O_0. At the moment, the moving coordinate system at the initial point is coincided with the absolute coordinate system, namely origin coordinate is acquired, so as to utilize transformation matrix to realize the shape of FBG flexible linear curvature's detection unit, further integrate coordinate data of all coordinate system, and realize deformation of model framework structure and vibrating morphological reconstruction.

$$\begin{cases} x = \dfrac{\sin(s_n \bullet \sqrt{\rho_{ny}^2 + \rho_{nz}^2})}{\sqrt{\rho_{ny}^2 + \rho_{nz}^2}} \\ y = [\dfrac{1}{\sqrt{\rho_{ny}^2 + \rho_{nz}^2}} - \dfrac{\cos(s_n \bullet \sqrt{\rho_{ny}^2 + \rho_{nz}^2})}{\sqrt{\rho_{ny}^2 + \rho_{nz}^2}}]\cos\theta_{ny} \\ z = [\dfrac{1}{\sqrt{\rho_{ny}^2 + \rho_{nz}^2}} - \dfrac{\cos(s_n \bullet \sqrt{\rho_{ny}^2 + \rho_{nz}^2})}{\sqrt{\rho_{ny}^2 + \rho_{nz}^2}}\sin\theta_{ny} \end{cases} \tag{7}$$

The implementation methods can be realized through the following steps:

Step one: The relative coordinate of the measure point in moving coordinate system is calculated.

Assuming that two orthogonal curvature of the measure point is ρ_{ny}, ρ_{nz} . The corresponding arc length is s_n, and then Formula (7) can be utilized to calculate the coordinate $P_n^t(x, y, z)$ of the measure point's moving coordinate system;

$$\theta_{ny} = \begin{cases} \arcsin \dfrac{\rho_{nz}}{\sqrt{\rho_{ny}^2 + \rho_{nz}^2}} & \rho_{\mathrm{ny}} \geq 0 \\ \pi - \arcsin \dfrac{\rho_{nz}}{\sqrt{\rho_{ny}^2 + \rho_{nz}^2}} & \rho_{\mathrm{ny}} < 0 \end{cases} \tag{8}$$

Step 2: The absolute coordinate under the fixed coordinate system can be calculated:

Assuming that the moving coordinate system of the point can be acquired through the operation of $R_n(x, y, z)$ and $P_{n-1}(x, y, z)$. $R_n(x, y, z)$ refers to the rotation of the coordinate system, $P_{n-1}(x, y, z)$ refers to the translation of the coordinate system, $P_{n-1}(x, y, z)$ refers to the coordinate value of the former point in the fixed coordinate system, and they satisfy the following boundary conditions as shown in Formula (9):

$$\begin{cases} P_0 = (0,0,0) \\ R_1 = (1,0,0) \end{cases} \tag{9}$$

Through the formula (10), $P_n(x, y, z)$ can be obtained:

$$P_n = \{[P_n^t \bullet A_x(-\theta_y) \bullet A_z(\theta_x)]\} \bullet A_x(\theta_y) + P_{n-1} \tag{10}$$

$A_x(\theta_x)$ refers to the matrix that a point rotates θx along z axle. θ_x and θ_y are acquired from Formula (11) and formula (12):

$$\theta_x = \arccos \frac{x_{R_n^1}}{\sqrt{x_{R_n^1}^2 + y_{R_n^1}^2 + z_{R_n^1}^2}} \tag{11}$$

$$\theta_y = \begin{cases} \arcsin \dfrac{z_{R_n^1}}{\sqrt{x_{R_n^1}^2 + y_{R_n^1}^2 + z_{R_n^1}^2}}, y_{R_n^1} \geq 0 \\ \pi - \arcsin \dfrac{z_{R_n^1}}{\sqrt{x_{R_n^1}^2 + y_{R_n^1}^2 + z_{R_n^1}^2}}, y_{R_n^1} < 0 \end{cases} \tag{12}$$

Where, R_n^t is calculated from Formula (13):

$$\begin{cases} x = \dfrac{\dfrac{1}{\sqrt{\rho_{ny}^x + \rho_{nz}^2}} - \dfrac{\cos(s_n \bullet \sqrt{\rho_{ny}^x + \rho_{nz}^2})}{\sqrt{\rho_{ny}^x + \rho_{nz}^2}}}{\tan(S_n \bullet \sqrt{\rho_{ny}^x + \rho_{nz}^2})} \\ y = y_{p_n^t} \\ z = z_{p_n^t} \end{cases} \tag{13}$$

Step 3: Update rotary operation of the next point, namely $R_n(x, y, z)$ is obtained from formula (14):

$$R_n = \{[R_n^t \bullet A_x(-\theta_y) \bullet A_z(\theta_x)]\} \bullet A_x(\theta_y) \tag{14}$$

5. FBG Sensor Network Optimization Layout Method

The modal displacement superposition method adopts the idea of finite element method to realize planar structure reconstruction. The sensor optimization layout in essence is an optimal combinatorial problem, namely specific measure point N should be selected from all finite element node M to enable to obtain the best reconstruction effect of planar structure under the combination.

Main constraint criteria of sensor optimization layout include:

(1) Demand constraint: Sensor number plays an important influence on the reconstruction effects. Theoretically, the more sensors there are, the better the reconstruction effect will be. In practical experiment, sensor number is selected as N=50 in line with FBG analyzer channel number and the number configuration constraint of every channel sensor, namely orthogonal measure point is 25.

(2) Interval constraint: In order to avoid from repeatability of measured strain information, the interval between every two measure points should be certain. In

actual experiment, the interval of any two sensors should not be less than 2 finite unit intervals, namely 4 cm.

(3)Reconstruction MSE constraint: $a(t)$ stands for estimation displacement, $a(t)^{'}$ stands for actual displacement, and reconstruction MSE is defined as:

$$E_{PMS} = \sqrt{\frac{\sum_{t=1}^{M} a(t-a(t)^{'})^{2}}{M}} \tag{15}$$

When E_{PMS} is the minimum, it means that the layout scheme is optimal. Thus, E_{PMS} is an important target of layout optimization.

(4)The same Row/rank constraint: The position of sensor measure point is set up as: $X_i(x_i, y_i)(i=1,2,\cdots,n)$. According to calculation characteristics of algorithm, in order to make row/rank layout points convenient for curvature data interpolation, sensor measure points should be stipulated in the same row or rank. If a rank sets up M measure points, a total of N ranks are arranged, and the same row and rank constraint can be expressed as formula (16):

$$f_1 = \sum_{i=1}^{M} |x_i - x_1| + \sum_{i=1}^{N} |y_m - y_1| \tag{16}$$

When solving optimized problems, a particle is corresponding to the solution of a problem. Particle information can be expressed as D-dimensional vector. The position is expressed as $X_i(x_{ii}, x_{i2}, \cdots, x_{iD})(i=1,2,\cdots,n)$. The velocity is $V_i(v_{ii}, v_{i2}, \cdots, v_{iD})(i=1,2,\cdots,n)$. Historical optimal position of the particle i is $P_{id}(p_{ii}, p_{i2}, \cdots, p_{iD})(i=1,2,\cdots,n)$, and historical optimal position of groups is $P_{gd}(p_{gi}, p_{g2}, \cdots, p_{gD})(i=1,2,\cdots,n)$. The velocity and position location update is shown as follows:

$$v_{id}(t+1) = wv_{id}(t) + c_1 r_1 (P_{id}(t) - x_{id}(t)) + c_2 r_2 (P_{gd}(t) - x_{id}(t)) \tag{17}$$

$$x_{id}(t+1) = x_{id}(t) + v_{id}(t+1) \tag{18}$$

r_1 and r_2 are the random number between [0, 1]; c_1 and c_2 is acceleration coefficient(is also called as learning factor) and regulate the biggest step towards overall optimal particle and individual optimal particle, respectively. If it is too small, the particle may be far from the target area; if it is too large, it may fly to the target area suddenly and fly over the target area. Generally speaking, $c_1 = c_2 = 1.5$; $w(t)$ is the inertia weight

and controls search range of particles. Based on the optimized algorithm of groups, initial optimization should encourage particles to move in the entire search range. In this way, it is beneficial for algorithm to do overall search. With the increase of iterations, particles are gradually restrained as the optimal adaptive value. The inertia weight should be reduced to look for the optimal solution accurately, so $w(t)$ is defined as:

$$w(t) = w_{\max} - (w_{\max} - w_{\min})(\frac{t}{MaxDT})^2 \tag{19}$$

In the formula (18), w_{max} is the maximum of inertia weight, and wmin is the minimum of inertia weight. *MaxDT* is the maximum iterations. Nonlinearity of $w(t)$ is gradually reduced and is more beneficial to obtain optimal solution. In order to prevent particles from flying out the boundary or fusing at the port, maximum velocity of particles can be restrained. Meanwhile, changes of particle position can be changed into circular changes, as shown in formula (20) and formula (21).

$$v_{id} = \begin{cases} v_{\max} & if \ \mathrm{v_{id}} > \mathrm{v_{max}} \\ -v_{\max} & if \ \mathrm{v_{id}} < \mathrm{-v_{max}} \end{cases} \tag{20}$$

$$x_{id} = \begin{cases} x_{id} - x_{\max} & if \ \mathrm{x_{id}} > \mathrm{x_{max}} \\ x_{id} + x_{\max} & if \ \mathrm{x_{id}} < 0 \end{cases} \tag{21}$$

When solving the optimization problem specially, the algorithm is conducted in line with the process shown in the Fig. 6.

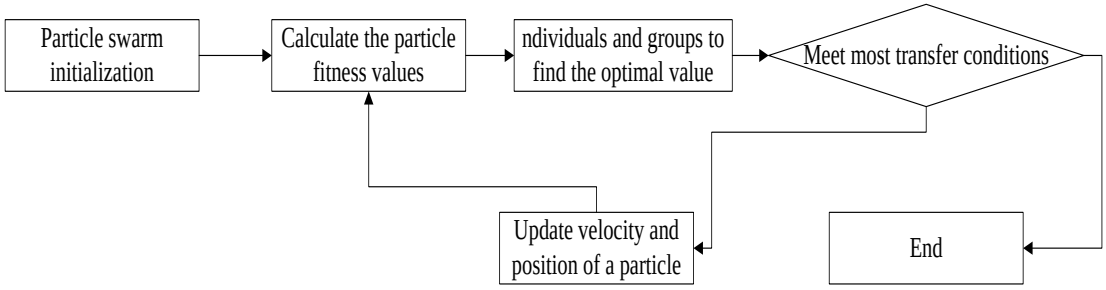

Fig. 6 Basic Algorithm Processes of Particle Groups

6. Empirical Analysis of Intelligent Structure Morphological Perception Sensor Monitoring

The specific experiment process is shown as follows: Signal generator outputs signal stimulus to the vibration exciter. Vibrational excitation makes experimental model structure generate deformation or enter into low-frequency vibration state. Experimental model structure deformation or vibration response information is perceived by FBG unit. Perceptive signal input and collection enter into FBG network analyzer, so as to realize acquisition of strain information at the measure point of experimental model structure distribution; Meanwhile, output data signal of FBG network analyzer is connected to a computer, which will do algorithm operation and graphic processing and display it on the display, so as to realize real-time perceptive construction and visualization display of experimental model structure deformation state or vibration state.

Aiming at experimental model structure of stimulated aircraft and based on experimental platform and software environment, real-time perception and reconstruction experimental verification of low-frequency structure vibration form are conducted, so as to verify dynamic characteristics of reconstruction algorithm and spot visualization effects. The experimental process is conducted within the 5-50Hz range of structure excitation frequency and emphasizes on structural vibration morphological structure state under vibration mode. The experimental process is shown as follows:

(1) Launch FBG analyzer and ensure normal hardware and software of experimental environment;

(2) Remote computer operation enables FBG analyzer to collect data; data servicer starts to acquire data and algorithm procedure starts to process data and render pictures;

(3) Regulate signal generator, set up output frequency and output amplitude; amplitude is generally set up as 2V; launch signal generator signal to generate;

(4) Regulate power output of power generator and enable vibration generator to generate obvious vibration for models;

(5) Observe visualized reconstruction situation of experimental model framework—girder construction, read reconstruction frequency, cut off experimental pictures, record data, conduct an experiment in line with experimental steps repeatedly under the vibration conditions of 5Hz, 10Hz, 20Hz, 30Hz and 50Hz, and the corresponding experimental data are shown in Table 6.3.1.

Table 1

Dynamic Experiment Effect Records of Framework

Vibrational frequency(Hz)	Observation of Reconstruction Effects
5	Obvious vibrational morphological reconstruction effects
10	Obvious vibrational morphological reconstruction effects
20	Obvious vibrational morphological reconstruction effects
30	Obvious vibrational morphological reconstruction effects
40	Unobvious vibrational morphological reconstruction effects
50	Unobvious vibrational morphological reconstruction effects

It can be observed from record data that when the vibration frequency of the experimental model structure is lower than 40Hz, the reconstruction algorithm can track the vibration response of the frame beam structure in real time, and can reflect its vibration form.

7. Experimental Results Analysis

By solving the mean square error between the offset of the grating measuring point in a certain direction and the calculated theoretical offset in a certain time range, the vibration morphological reconstruction of the structural vibration form is obtained. as shown in formula (22):

$$\begin{cases} E_{RMS}(t) = \dfrac{\sqrt{\dfrac{\sum_{i=1}^{n}(w_i(t) - \hat{w}(t))}{n}}}{w_{\max}} \times 100\% \\ E_{RMS} = \max(E_{RMS}(t)) \end{cases} \tag{22}$$

w represents the actual offset measurement of the raster measurement point, $w_{\max}$ represents the maximum amplitude, $\hat{w}$ represents the theoretical calculated value, n represents the number of grating measurement points, E_{RMS} is the maximum value of the offset for each measurement point within the measurement time, Table 2 shows the relative root mean square error of the measurement points at different excitation frequencies.

Table 2

The relative mean square error of the measuring point is measured by different excitation frequency

Excitation frequency (Hz)	**5**	**10**	**20**	**30**
RMS error (%)	0.82	1.28	1.72	2.75

As can be seen from Table 2, when the excitation frequency of the model structure is lower than 30Hz, the RMS error value of vibration morphological reconstruction is small.

Conclusions

Intelligent surface structure is a multi-disciplinary research field of high technology, which has important research significance and good application prospects, but also constitutes a hot spot in the field of smart structures at home and abroad. This article has carried on the positive exploration and the thorough research in this domain. The optimized discrete FBG sensor network is constructed and the feasibility of the optimization algorithm and the effectiveness of the optimization result are verified by experiment and calculation. Based on the orthogonally discrete FBG sensor network, the flexible plate shape morphological perception and reconstruction method can realize the real-time perception and reconstruction of statistical morphological changes and vibrational morphological changes at frequencies below 30Hz vibration frequency. The reconstruction method not only enriches the traditional structure monitoring and diagnosis technology, but also has wide application prospect in engineering practice, such as damage detection of sailing hull, monitoring of deformation, monitoring of tunnel deformation, monitoring of road disaster, slope deformation Monitoring, aerospace and other fields.

Acknowledgements

The authors would express their appreciation for the financial support of Shandong Natural Science Foundation, grant NO. ZR2011EL016. The authors also would express their thanks for Shandong Science and Technology Development Project on Safety in Production, grant NO. LAJK2013-183.

R E F E R E N C E S

[1] *Liu Weibo and Zhang Xiaopeng,* Non-linear Discussion of Displacement Sensor in Ice Mechanical Testing, Journal of Dalian University of Technology, 2000, 40(3); 285-288

[2] *Guo Mingjin and Jiang Desheng, etc.,* Low-Temperature Characteristics of Naked FBG and Closed FBG, Journal of Wuhan University of Technology, **Vol**.8, 2006, pp8-9

[3] *Zhang Dan, Shi Bin and Wu Binshen, et al.,* BOTDR Distributed FBG and its Application in Structural Health Monitoring, Journal of Civil Engineering, **Vol**.36 (11), 2003, pp 83-87

[4] *Deng Jiangang , Guo Tao, Xu Qiuyuan, Nie Dexin, Cheng Zao and Cheng Lin,* "Design and Performance Test for Fiber Bragg Grating Sensors of Transformer Winding Temperature Measurement", High Voltage Engineering, **Vol.**38, No.6, June 30, 2012, PP.1348-1355.

[5] *Davis,D. D., Gaylord, T. K., Glytsis, E. N., Kosinski,S. G., Mettler，S. C. and Vengsarkar,A. M.,* "Long-period Fibre Grating Fabrication with Focused CO2 Laser Pulses", Electronics Letters, **Vol**. 34, No. 3, 1998, pp. 302-303.

[6] *Meltz G, Morey WW and Glenn WH,* "Formation of Bragg Gratings in Optical Fibers by A Transverse Holographic Method", Optics Letters, **Vol**. 14, No. 5, 1989, pp.823-825.

[7] *Jin Yongxing, Liu Tao, Fang Tao, Kang Juan and Shen Weimin,* "Experimental Study of Temperature Sensor Systems for FBG based on LabVIEW", Laser Journal, **Vol**. 30, No. 1, 2009, pp 32-33.

[8] *Zhou Yuqing, Mei Xuesong and Jiang Gedong et al.,* Large-Scale Numerically-controlled Machine Tool Based on Built-in Sensor, Journal of Mechanical Engineering, **Vol**.45(4), 2009, pp. 125-130

[9] *Jiang Deshan, Fan Dian and Mei Jiachun,* Multiplexing Based on FBG Sensor, Progress of Laser and Optoelectronics, **Vol**. 42(4), 2005, pp.14-19

[10] *N. Takeda, S. Minakuchi, Y. Okabe.* Smart Composite Sandwich Structures for Future Aerospace Application-Damage Detection and Suppression: A Review. Journal of Solid Mechanics and Materials Engineering, **Vol.** 1 (1), 2007, pp 3-17

[11] *Huang Minshuang, Liang Dakai and Yuan Shenfang et al.,* FBA New Technology Study Based on Intelligent Structure, Journal of Aviation, **vol**. 22(4), 2001, pp. 326-329

[12] *A. S. Guru Prasad, M. Anitha, K. S. Nanjunda Rao and S. Asokan,* "Measurement of Stressstrain Response of A Rammed Earth Prism in Compression Using Fiber Bragg Grating Sensors", International Journal on Smart Sensing and Intelligent Systems, **Vol**. 4, No. 3, September 2011, pp 376-387.

[13] *K. O. Hill, Y. Fujii, D. C. Johnson and B. S. Kawasaki, "*Photosensitivity in Optical Fiber Waveguides: Application to Reflection Filter Fabrication", Applied Physics Letters, **Vol**. 32, No.10, 1978, pp. 647- 649.

[14] *T. Erdogan and J.E. Sipe,* "Tilted Fiber Phase Gratings", Journal of the Optical Society of America A, **Vol**. 13, No. 82, 1996, pp. 296-313.

[15] *Dennis Snelders and Arjen Boersma,* "Development of Thermostable FBG Optical Sensor for Oil and Gas Applications", Proceedings of the 8th International Conference on Sensing Technology, Sep. 2-4, 2014, pp. 278-281.

[16] *Xixin Jiang, Zude Zhou and Guangrong Bian,* "A Rotating Cantilever Beam for Dynamic Strain Measurement and Vibration Analysis Based on FBG Sensor ", International Journal on Smart Sensing and Intelligent Systems, **Vol**. 6, No. 5, 2013, pp. 2277-295.

[17] *Haidou Yang and Wei Li,* "Performance Measurement of Photoelectric Detection and Target Tracking Algorithm", International Journal on Smart Sensing and Intelligent Systems, **Vol**. 8, No. 3, 2015, pp. 1554 – 1575